ESO 137-002: a ram-pressure-stripping galaxy but not a jellyfish galaxy with a star forming tail

Sunil Laudari[1]⋆, Pavel Jáchym[2]†, Ming Sun[1]‡, Will Waldron[1], Marios Chatzikos[3],
Tim Edge[1], Rongxin Luo[1], Jeffery Kenney[4], Craig Sarazin[5], Mark Voit[6],
Megan Donahue[6], Paul Nulsen[7,8], Françoise Combes[9], Luca Cortese[8] (order TBD)

[1]*Department of Physics & Astronomy, University of Alabama in Huntsville, 301 Sparkman Dr NW, Huntsville, AL 35899, USA*
[2]*Astronomical Institute, Academy of Sciences of the Czech Republic, Boční II 1401, 141 31 Prague 4, Czech Republic*
[3]*Department of Physics & Astronomy, University of Kentucky, Lexington, KY 40506, USA*
[4]*Yale University Astronomy Department, P.O. Box 208101, New Haven, CT 06520-8101, USA*
[5]*Department of Astronomy, University of Virginia, Charlottesville, VA 22904, USA*
[6]*Department of Physics and Astronomy, Michigan State University, East Lansing, MI 48824, USA*
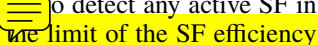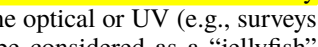[7]*Harvard-Smithsonian Center for Astrophysics, 60 Garden Street, Cambridge, MA 02138, USA*
[8]*ICRAR, University of Western Australia, 35 Stirling Hwy, Crawley, WA 6009, Australia*
[9]*Observatoire de Paris, LERMA, PSL, CNRS, Sorbonne Univ. UPMC, and College de France, F-75014, Paris, France*

ABSTRACT

Ram pressure stripping (RPS) is an important mechanism for galaxy evolution. Many examples of RPS galaxies have been revealed recently. In this work, we present results from the *HST* and *APEX* observations of one RPS galaxy ESO 137-002 in the closest rich cluster Abell 3627. The galaxy is known to host prominent X-ray/Hα tails. The *HST* data reveal significant features indicative of RPS in the galaxy, including asymmetrical distribution of dust in the galaxy, dust filaments and dust clouds in ablation generally aligned with the direction of ram pressure, and young star clusters immediately upstream of the residual dust clouds. Some young star clusters are found in the galaxy and we argue the SF is triggered by ram pressure compression. Our CO data from *APEX* also reveal an asymmetrical distribution of the molecular gas in the galaxy, with no CO detection in the upstream and abundant CO in the downstream. CO emission is also detected from the near tail region. A total amount of $\sim 5.5 \times 10^{10}$ M$_\odot$ of molecular gas is detected from the galaxy and its tail. On the other hand, we also detect any active SF in the X-ray/Hα tails of ESO 137-002 with the *HST* data and set the limit of the SF efficiency in the tail. Hence, if selected by SF tails behind the galaxy in the optical or UV (e.g., surveys like GASP or using the *Galex* data), ESO 137-002 will not be considered as a "jellyfish" galaxy. Thus, the inclusion of galaxies like ESO 137-002 is important for our comprehensive understanding of RPS galaxies and the evolution of the stripped materials.

Key words: galaxies: individual: ESO 137-002 – galaxies: clusters: individual: Abell 3627 – galaxies: evolution – galaxies: star clusters: individual: star formation — galaxies: interactions

1 INTRODUCTION

Galaxy clusters are the largest gravitationally bound structures in the universe, filled with hot diffuse plasma with a typical temperature of $10^7 - 10^8$ K and electron number density of $10^{-4} - 10^{-1}$ cm^{-3} (Voit 2005; Kravtsov & Borgani 2012). They contain a large fraction of Es/S0s mostly concentrated around the cluster core and with a relatively small fraction of spirals/irregulars. Cluster galaxies are pref-

erentially red with little cold gas and suppressed star formation (SF) activities (e.g., Dressler 1980; Poggianti et al. 2006). Conversely, field galaxies are mostly spirals that are preferentially blue, exhibit more cold gas, and have active SF activities. These characteristics suggest galaxy evolution is strongly influenced by their environments. Several mechanisms like galaxy harassment (Moore et al. 1998), starvation (Larson et al. 1980), galaxy—galaxy interaction (Sulentic 1976; Kapferer et al. 2005), ram pressure stripping (RPS) (Gunn & Gott 1972), viscous stripping (Nulsen 1982), evaporation (Cowie & McKee 1977) and galactic winds (Mathews & Baker 1971) have been proposed to explain the transformation of galaxy

---

⋆ E-mail: ming.sun@uah.edu
† E-mail: jachym@ig.cas.cz
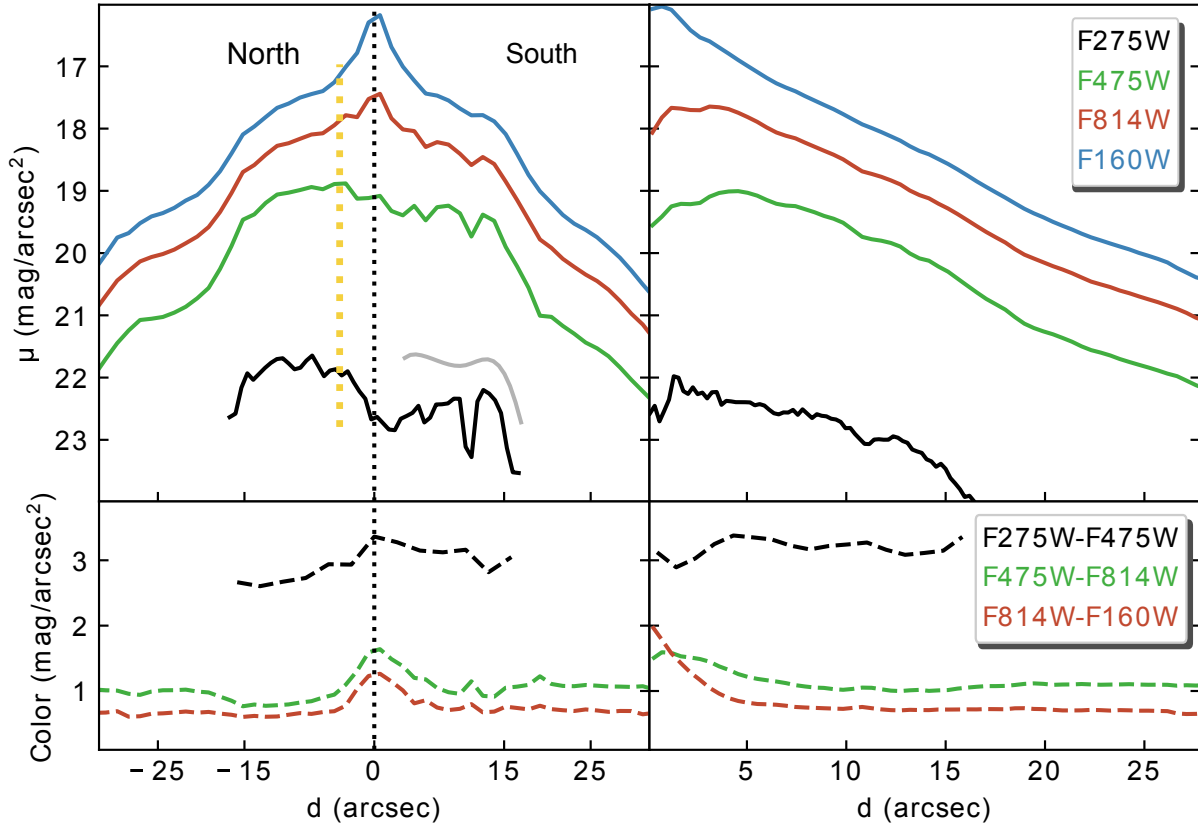‡ E-mail: ming.sun@uah.edu

Figure 4. The surface brightness profiles measured along the major axis (*Upper Left*, with $d = 0$ at the nucleus) and the elliptical annuli centered at the nucleus (*Upper Right*, a as the semi-major axis), in all four bands. The color profiles are shown in the lower panel. The elliptical annuli have a PA of -14.01° and an axis ratio 0.256. One can observe the significant effect of dust extinction at short wavelengths, while the F160W (or H-band) profiles are smoother and more symmetric than the profiles of the other three bands. As shown in Fig. 1, the F275W light truncates at ∼ 16″ from the nucleus. The yellow dashed line marks the position of the stripping front. The grey profile in the upper left panel is the downstream F275W profile after correction of the intrinsic extinction with the F475W and F814W data (see Section 4.2 for detail), which suggests that the galaxy would have been more symmetric in F275W without the intrinsic extinction (see Fig. 1).

Table 4. GALFIT fits on the F160W image of ESO 137-002

Parameter	Single (χ_ν^2=5.693)	Double (χ_ν^2=2.025)	
		Bulge	Disk
Total magnitude (mag)	11.53	12.49	12.12
r_e (kpc)	4.09	2.05	5.17
Sérsic index	1.41	2.43	0.74
Axis ratio	0.23	0.66	0.13
Positional angle (deg)	-13.1	-13.9	-13.3

Note: The axis ratio is the ratio between the minor axis and the major axis. The position angle is measured relative to the north and counter-clockwise.

4.2 Dust Features

To better show the dust features in the galaxy, we applied unsharp masking on the F475W image, by subtracting the original image smoothed with 1 pixel from the same image smoothed with 20 pixels (Fig. 5). It shows many dust features around the nucleus and downstream, extending to at least 13.5 kpc to the SE. A prominent dust lane is observed around the nucleus and there are many dust filaments and clouds downstream.

We also used GALFIT again to produce a smooth model of the galaxy, this time on the F475W image. The final GALFIT model has four Sérsic components, two in the disk and two in the bulge, along with the Fourier modes (mode= 4, 6 and 8). The residual image is shown in the middle panel of Fig. 5. It should be noted that the dark features upstream of the galaxy are from over-fitting and not caused by dust. We also highlighted dust features in zoom-in insets. Inset a) shows the strong dust lane in the bulge, with the nucleus buried in the position with the strongest dust extinction. Inset b) goes further downstream and encloses an interesting 'X'-shaped feature with a length of ∼ 0.8 kpc. Inset c) shows numerous dust threads, arcs and filaments further downstream, to at least 13.5 kpc from the nucleus. These dust threads have a typical length of ∼ 0.8 kpc and width of ∼ 0.1 kpc, which can be compared with dust filaments in the leading edge of NGC 4921 with 0.5 - 1 kpc in length and 0.1 - 0.2 kpc in width. The dust filaments in the downstream are roughly aligned with the RPS direction, determined from the X-ray/Hα tails. This reflects the effect of RPS on dust ablation from dense ISM clouds. The orientation of these dust filaments may also be affected by magnetic field and disk rotation in ESO 137-002. The significance of these dust features also suggests that they mostly lie in the front side of the galaxy. The existence of long, coherent dust filaments suggests that magnetic field plays an important role here. If a similar dust-to-gas ratio as in the Milky Way is assumed (Güver & Özel 2009), the H I + H$_2$ column density of the strongest dust filament is ∼ 13.7 M$_\odot$ pc^{-2} at the downstream region.

To quantify the dust extinction in the galaxy, we derive the E(B-V) map of the galaxy, with the F475W and F814W data. A key assumption in this analysis is that the F475W - F814W color of the galaxy is symmetric around the nucleus. Since the upstream
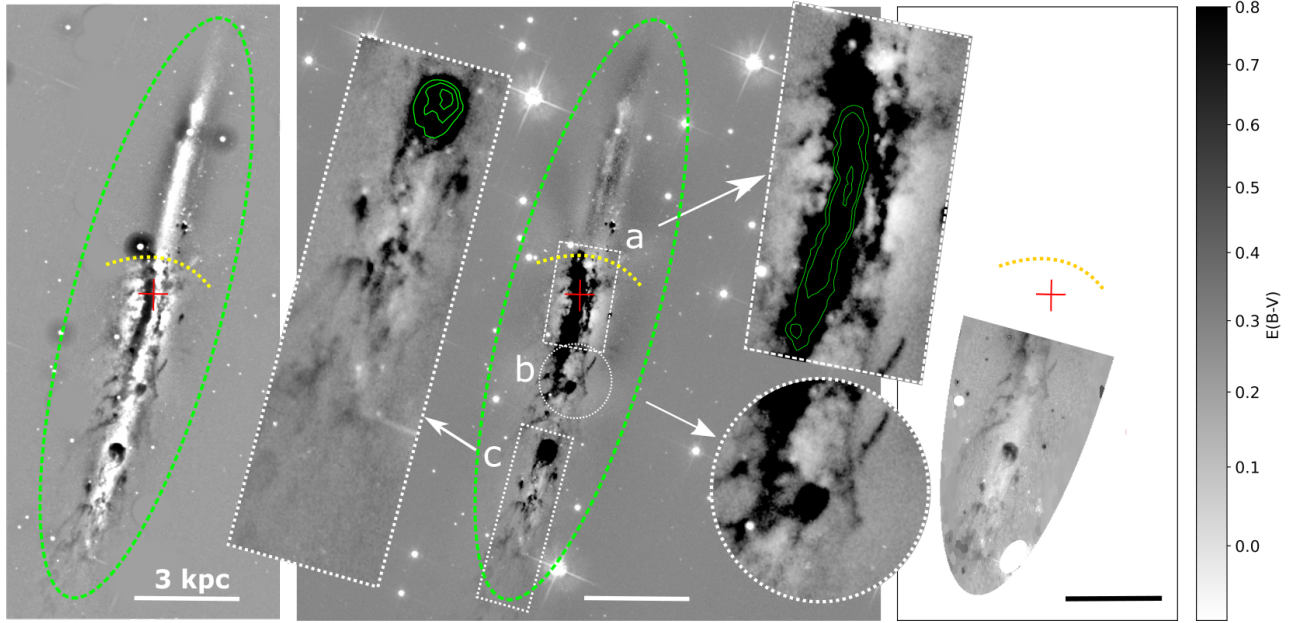
Figure 5. *Left*: The unsharp masked F475W image of ESO 137-002, after subtracting the original image smoothed with 1 pixel (or 0.03″) from the same image smoothed with 20 pixels. Prominent dust lanes and filaments are visible which extend from the nucleus/bulge to the downstream or the SE direction. The red cross shows the position of the nucleus (the same for the other two panels) and the green ellipse shows the region of the E(B-V) image on the right (the same for the middle panel). The yellow arc in the dashed line is the same stripping front as shown in Fig.3 (also the same for the other panels). *Middle*: the residual F475W image, after subtracting the GALFIT model image obtained with four Sérsic components with the Fourier mode (see Section 4.2). Similar dust features as shown on the left are also visible in this residual image and highlighted in zoom-in panels from a to c (the dark features upstream are from over-subtraction instead of dust features). Inset a) shows the main dust lane around the nucleus, with the green contours show the levels of deficits. Inset b) shows some dust filaments trailing the SE of the nuclear region. Inset c) shows a large dust cloud (with a radius of ∼ 0.22 kpc) in the middle of downstream (green contours also show the levels of deficits), as well as many dust clouds and filaments further downstream that can be traced up to ∼ 13.5 kpc from the nucleus. *Right*: The E(B-V) map derived from the F475W and F814W images, assuming that the upstream region is dust free and an extinction law from Fitzpatrick (1999). The strongest extinction is around the nucleus and the large dust cloud in the middle of the downstream region (highlighted in the inset c in the middle panel).
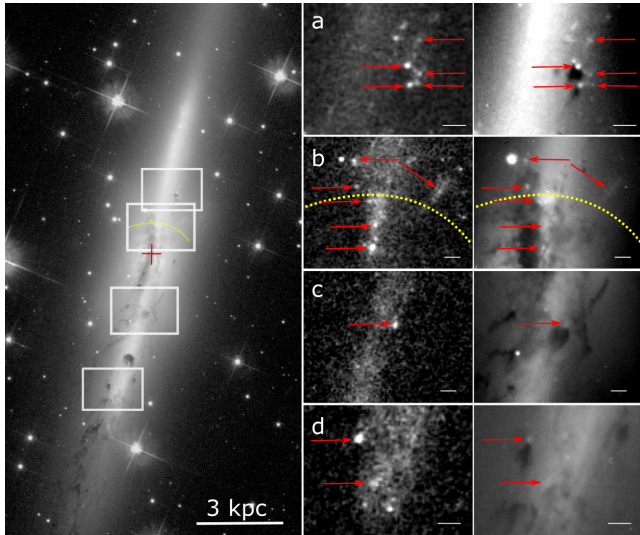

Figure 6. *Left:* The F475W image of ESO 137-002 with four white boxes to zoom in around young star clusters revealed in the F275W band. The stripping front is shown by the yellow arc (the same as in Fig.3). *Right:* The four zoom-in regions (a, b, c and d) to show the young star clusters in the disk (highlighted by red arrows) in the F275W (*left*) and F475W (*right*) images. These young star clusters are bright in F275W but faint in red bands. Some are located immediately upstream of dusty clouds, which implies that the SF there was triggered by the compression from ram pressure. The white scalebar in each small panel is 0.2 kpc.

4.4 Nucleus

ESO 137-002's nucleus hosts an obscured AGN from the X-ray data (Sun et al. 2010; Zhang et al. 2013). The nuclear position is determined from the *Chandra* data, at (16:13:35.763, -60:51:54.74) with an uncertainty of ∼ 0.5″. The *HST* data reveal that the nuclear region is indeed heavily obscured by dust. The average E(B-V) values around the nucleus is ∼ 0.5. It is unclear whether the RPS in ESO 137-002 has anything to do with its active nucleus (e.g., Poggianti et al. 2017). MS revised it on 06/24/20; likely need to add a bit more description/analysis in the future

5 *HST* SOURCE POPULATION IN THE TAIL

We also want to examine the source population in the X-ray/Hα tail and search for young star clusters as found in many "jellyfish" galaxies. As shown in Fig. 2, we defined three regions of interest to characterize sources — galaxy, tail and control regions. The tail region encloses the X-ray and Hα tails as shown in Zhang et al. (2013). The choice of the control region is mainly determined by the common FOV between the F275W and the F475W data. The galaxy region encloses sources in the galactic disk.

Source detection and aperture photometry were again performed in all bands with SExtractor, with an aperture radius of 0.5″. The F475W data were used as the detection. Before the final color - color and color - magnitude diagrams, we filtered out spurious sources, weak sources, very red sources and foreground
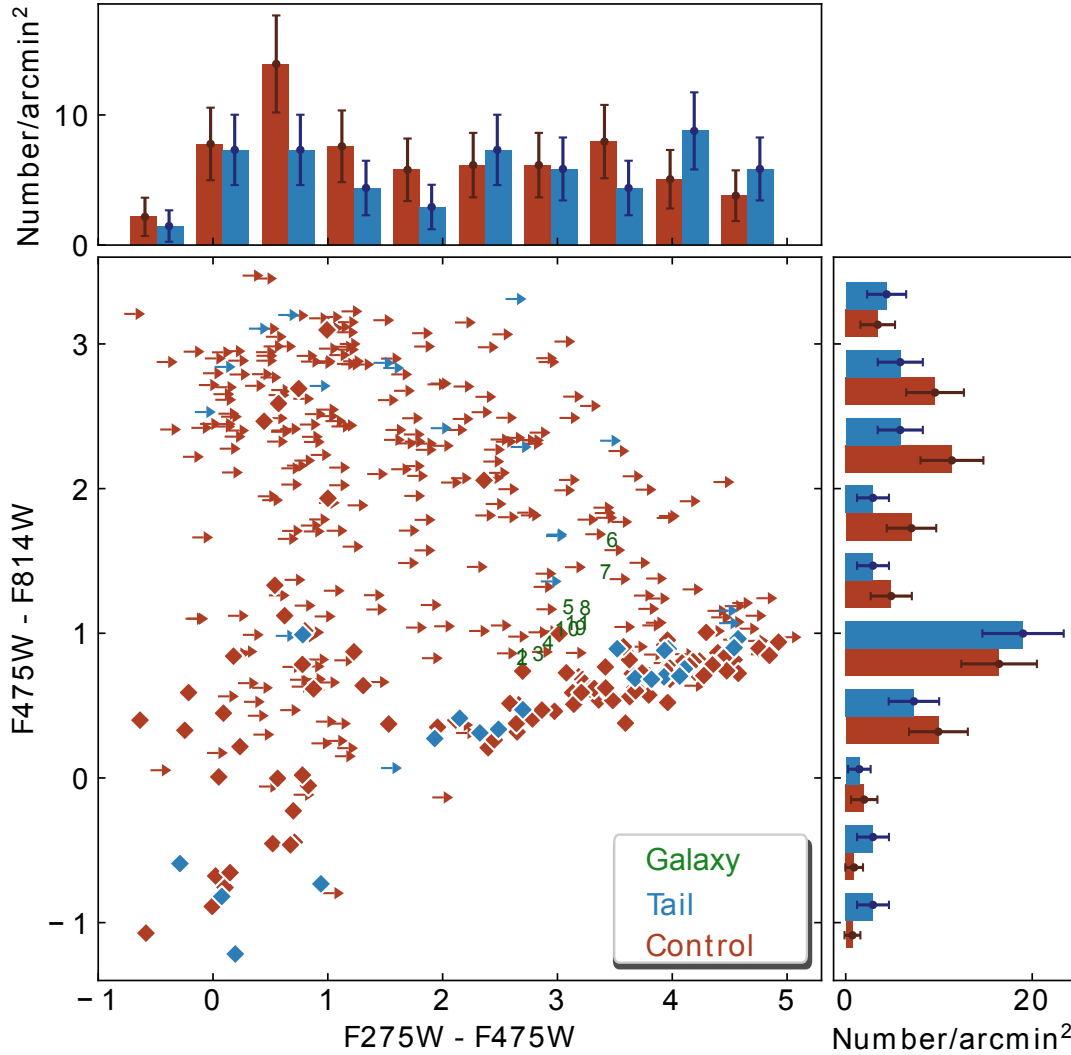
Figure 8. The color-color diagram for sources detected in F275W, F475W and F814W (diamonds) and sources only detected in F475W and F814W (arrows), in tail (blue) and control (red) regions. The initial detection was made in F475W. Most sources are undetected in F275W so F275W − F475W colors are mostly limits. The tail/control regions are the regions in lightblue and grey respectively in Fig. 2. The source selection is discussed in Section 5. Colors of the galactic disk are again shown in green numbers as in Fig.7. The median F475W − F814W errors are 0.02 mag and 0.06 mag for the tail and control regions respectively. The histograms are normalized to the region area (0.684 arcmin² for the tail region and 5.532 arcmin² for the control region). Error bars of the source counts are also plotted. As the distributions of both colors in the tail region are consistent with those in the control region, there is no evidence of young star clusters in the tail region.

of 0.8, the corresponding molecular gas mass in the 002-C region is about $4.4 \times 10^9 M_\odot$. The formula includes a factor of 1.36 to account for the effects of Helium. We assume a typical CO(3-2)/CO(1-0) ratio of 0.6 (Mao+2010...).

A Gaussian fit to the 002-C CO(2-1) line (shown in Fig. 11) has a width of ~ 430 km s^{-1} which is consistent with ESO 137-002's circular velocity of ~ 200 km s^{-1} that is estimated from the galaxy's K-band magnitude −24.3 (NED) and using the velocity-luminosity relation of Courteau et al. (2007). While the CO line seems to have a classical two-horned profile caused by the disk rotation, it is asymmetric with (a) more pronounced low-velocity side and (b) strong peak in the middle of the line. The former is likely due to pointing the APEX 002-C aperture about 1.4 kpc southwards off the (optical) galaxy center where it encloses more gas from the southern disk side that rotates towards the observer, i.e. at smaller

radial velocities. The latter may suggest existence of a gas with low radial velocity component relative to the galaxy, as the peak occurs at the galaxy's systemic radial velocity of 5585 km s^{-1} (assuming the radio definition of the velocity). Its origin is likely in a compact central source, such as a circumnuclear disk (e.g., Israel+1999). Many observations have shown that molecular gas is more centrally concentrated in galaxies with bars, suggesting that a bar can play an important role in gas-fueling toward the central region, thus feeding starbursts or AGN activities (Kuno et al. 2007). The average central gas surface density of barred spirals is known to be about three times higher than that of unbarred galaxies (Sheth+2004). ESO 137-002 indeed has a bar as discussed in Section 4.1 and it hosts a Seyfert-2-like nucleus (Sun et al. 2010; Zhang et al. 2013).
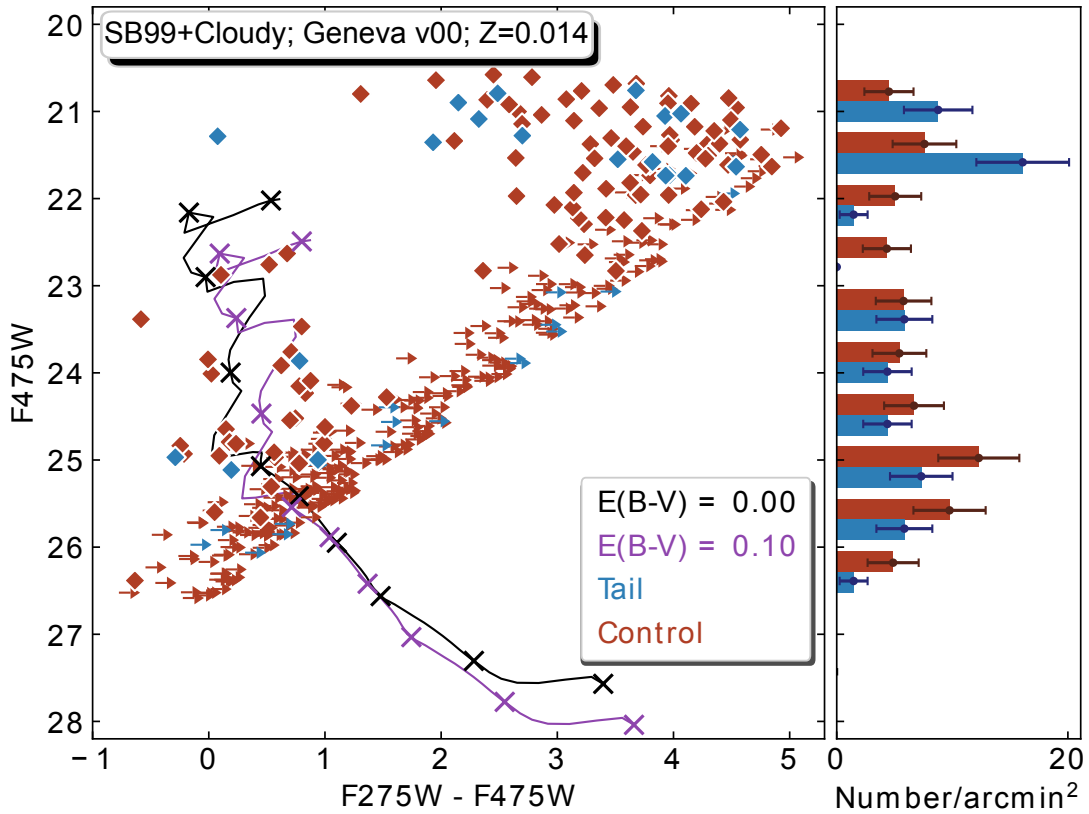
Figure 10. The F275W - F475W color — F475W magnitude diagram for sources detected in F275W, F475W and F814W (diamonds) and sources only detected in F475W and F814W (arrows), in tail (blue) and control (red) regions. The SB99 tracks (for a total mass of 10^4 M$_\odot$), with the nebular emission added from Cloudy simulations, are also shown with E(B-V) = 0 and 0.1. The markers on the track indicate ages of 1, 3, 5, 10, 30, 50, 100, 200, 500 and 1000 Myr starting from the blue end. A histogram on the source surface number densities in these two regions is shown on the right, which suggests no significant difference on the F475W magnitude distribution between sources in the tail and control regions. The somewhat higher number of bright sources in the tail region are almost all red ones (e.g., F275W - F475W > 1 mag). Combined with Fig. 8 and Fig. 9, the source population in the tail region has no significant difference from that in the control region and there is no evidence for active SF in the tail region.
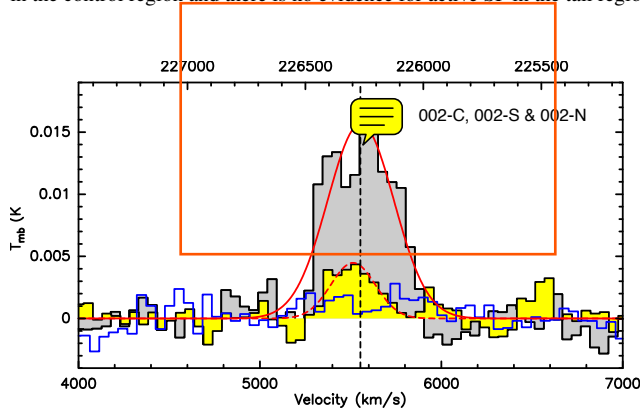

Figure 11. The CO(2-1) spectra of ESO 137-002 in the central pointing 002-C (grey), the southern off-center position 002-S (yellow), and the symmetrical northern position 002-N (blue). Spectra are smoothed to 50.8 km s^{-1} channels. Parameters of the Gaussian fits to the 002-C and 002-S lines are given in Table 5. The central velocity 5554 km s^{-1} of the fit in central point is shown with the dashed line. The systemic radial velocity of ESO 137-002 is 5585 km s^{-1} (assuming radio definition of the velocity).

6.2 Asymmetric CO distribution in the disk

To cover the continuation of the bright X-ray and Hα emission in the southern part of the disk, the 002-S APEX beam was pointed ∼ 7.8 kpc south from the optical disk center, adjacent to the 002-C region (see Fig. 2). A rather strong CO(2-1) line is detected with a S/N ∼ 12 at a resolution of 51 km s^{-1} (see Fig. 11). The corre-

sponding molecular gas mass is ∼ 1.0×10^9 $M_\odot$. The linewidth measured from a Gaussian fit is ∼ 302 km s^{-1}, by about 130 km s^{-1} less than in the central 002-C pointing. The line is asymmetric, with more emission coming from the low-velocity side, which is consistent with detecting the gas that is rotating towards the observer. The high-velocity wing of the line exceeds the galaxy's systemic radial velocity, suggesting that the kinematics of the gas in the southern disk part may be altered by the effects of ram pressure. However, contamination by the secondary beam lobes that may register emission from the receding (northern) disk side is also possible.

We further observed the region 002-N located in the northern, windward disk side, symmetrically to the southern 002-S pointing with respect to the optical center of the disk (see Fig. 2). No obvious line emission appears in the 002-N spectrum, down to a much higher sensitivity than in the 002-S point. From the measured rms noise σ_{rms} we calculate 3σ upper limit on the CO flux density

$$S_{CO} < 3\sigma_{rms} \sqrt{\Delta v_{CO} \, dv}, \qquad (5)$$

where dv is the channel size (52 km s^{-1}) and Δv_{CO} is the mean FWHM linewidth. Assuming a linewidth of 300 km s^{-1}, the rms corresponds to a mass sensitivity of ∼ 6.4×10^7 $M_\odot$. In the northern, windward part of the disk of ESO 137-002, there is thus at least 15-times less molecular gas than in its southern, leeward part. This indicates a strong asymmetry in the molecular component distribution in the disk, likely due to the effects of ram pressure stripping.
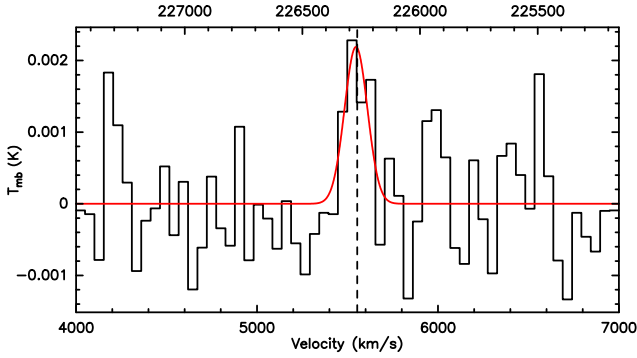
Figure 12. The CO(2-1) spectrum measured in the (inner) tail of ESO 137-002. Spectrum is smoothed to ∼ 50 km s^{-1} channels. Parameters of the Gaussian fits are given in Table 5. The central velocity of the line in the 002-C region is indicated with the dashed vertical line.

Figure 13. The CO(3-2) spectra measured in the central (grey) and southern (yellow) positions over ESO 137-002. Spectra are smoothed to ∼ 50 km s^{-1} channels. Parameters of the Gaussian fits are given in Table 5. The central velocity of the line in the 002-C region is indicated with the dashed vertical line. The spectrum of the central position is double-peaked with a velocity separation of ∼ 300 km/s.

6.3 Inner tail of ESO 137-002

We targeted another observation (002-T) to the region where mainly X-ray tail extends from the galaxy, already outside of the disk, about ∼ 15 kpc from its optical center (see Fig. 2). The integration was very deep and an rms sensitivity of 0.5 mK in 52 km s^{-1} channels was reached. Fig. 12 shows the spectrum with a gaussian fit of the detected $I_{CO}/\sigma_I \sim 7\sigma$ line. The FWHM of the line is considerably smaller than in the 002-S region - only ∼ 135 km s^{-1} (by about a factor of 2.2). The line luminosity corresponds to an H$_2$ mass of ∼ 1.3×10^8 $M_\odot$. At a smaller resolution, the spectrum suggests the line has a substructure, possibly reflecting emission from a set of GMCs. In another Norma cluster galaxy, ESO 137-001, large amounts of molecular gas were detected in the tail. Since ESO 137-002 is stripped (and observed) edge-on, the tail overlays with the disk, before it extends from the galaxy. In a face-on configuration, the tail is extra-planar. The 002-T region thus should be compared to the 001-tailB region in ESO 137-001, where about 3-times more H$_2$ was detected (Jáchym et al. 2014).

6.4 CO(3-2) emission and CO(3-2)-to-CO(2-1) line ratios

The central and southern regions of the ESO 137-002 disk were further observed in CO(3-2). The locations of the two pointings were slightly offset with respect to the CO(2-1) regions 002-C and 002-S in order to better cover the asymmetric X-ray and Hα emission with the smaller CO(3-2) beams (see Table 3 and Fig. 2). The corresponding CO luminosities and H$_2$ masses are given in Table 5. In the central region the CO(3-2) line is double-horned with some emission also at the central line velocity, similarly to the CO(2-1) 002-C line profile (see Fig. 13).

Following Eq. 3, the luminosity line ratios, $r_{32} = L'_{CO(3-2)}/L'_{CO(2-1)}$ in the two regions are 0.51 and 0.43, not corrected for different beam sizes (∼ 27″ vs. 17″). The galaxy is edge-on and it can be expected that most of the molecular gas is concentrated in the disk plane. Also the ram pressure operating on the galaxy is nearly fully edge-on. The difference in the beam sizes in the direction perpendicular to the disk-plane thus does not play much role and it is mostly the difference along the disk plane that matters. We thus simply apply a 1D geometrical beam correction factor of 26.7″/17.8″ = 1.5 that increases the r_{32} line ratios in the 002-C-CO32 and 002-S-CO32 regions to 0.77 and 0.65, respectively. A more precise way for calculating a beam correction factor would be to follow the assumption that the IR dust emission is a good tracer of the cold molecular gas and measure the flux within
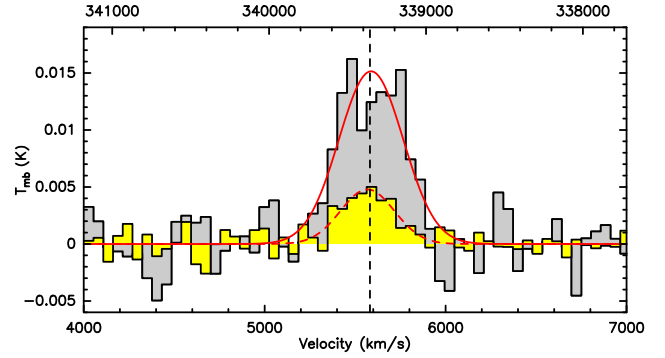
different apertures in the IR images. But this approach is beyond the scope of this paper.

In low-redshift normal star-forming galaxies, typical mean values of the CO line ratios are $r_{31} = 0.55 - 0.61$ (Saintonge et al. 2017; Mao et al. 2010), and $r_{21} = 0.79 - 0.81$ (Saintonge et al. 2017; Leroy et al. 2009). This translates to the typical r_{32} ratio of ∼ 0.7. Our measurements in the two regions in ESO 137-002 are thus consistent within uncertainties with the typical values in local star-forming galaxies. The luminosity line ratio can be interpreted as an indicator of the gas density. The critical density of the CO(3-2) transition calculated under the optically thin assumption is 3.6×10^4 cm^{-3}. The r_{32} line ratio may thus be considered a proxy for the ratio of relatively dense to more diffuse molecular gas. Many studies searched in galaxies for correlations between the CO line ratios and star formation rates or star formation efficiencies (SFE), finding that the r_{31} ratio tends to increase with SFE, suggesting that galaxies with a higher fraction of dense molecular gas tend to have higher SFE (e.g., Lamperti et al. 2020). Despite a large scatter in the correlation (see Fig. 3 in Lamperti et al. 2020), it is clear that the values of the line ratios measured in the two regions in ESO 137-002 should correspond to a larger SFE in a normal SF galaxy. In other words, despite its large amounts of molecular gas and the relatively large fraction of the denser molecular gas traced by the CO(3-2) emission, ESO 137-002 has a rather low SFE: SFE = SFR/$M_{H_2} \approx$ 0.89 $M_\odot$ yr^{-1}/5.5×10^9 $M_\odot$ ∼ 1.6×10^{-10} yr^{-1}. The effects of ram pressure of the surrounding ICM, as well as the active nucleus (i.e. a source of X-rays) of the galaxy, may be responsible for its measured low SFE.

7 DISCUSSION

7.1 Star formation in the galaxy

The total FIR luminosity of the galaxy was derived from the *Herschel* data. We used the *Herschel* source catalog, particularly the PACS Point Source Catalog and the SPIRE Point Source Catalog. We used the python code MBB_EMCEE to fit modified blackbodies to photometry data using an affine invariant Markov chain Monte Carlo (MCMC) method, with the *Herschel* passband response folded (Dowell et al. 2014). Assuming that all dust grains share a single temperature T_d, that the dust distribution is optically thin, and neglecting any power-law component towards shorter

wavelengths, the fit results in a temperature of $T_d = (27.8\pm0.2)$ K, a luminosity $L_{8-1000\,\mu m} = (1.22 \pm 0.02) \times 10^{10}$ L$_\odot$, and a dust mass of $M_d = (6.7 \pm 0.3) \times 10^6$ M$_\odot$ for $\beta = 1.5$. For $\beta = 2$, $T_d = (24.7\pm0.2)$ K, $L_{8-1000\,\mu m} = (1.21 \pm 0.02) \times 10^{10}$ L$_\odot$ and $M_d = (1.2 \pm 0.1) \times 10^7$ M$_\odot$. We also performed a fit using a free β parameter, which results in $T_d = 26.6^{+0.9}_{-0.7}$ K, $L_{8-1000\,\mu m} = (1.22 \pm 0.02) \times 10^{10}$ L$_\odot$, $M_d = 8.7^{+0.9}_{-1.6} \times 10^6$ M$_\odot$, and $\beta = 1.69^{+0.09}_{-0.14}$. With the measured FIR and CO luminosities, we can put ESO 137-002 in the well-known CO - FIR correlation (e.g., Solomon & Vanden Bout 2005) and its position is consistent with normal spirals on the relation.

The total SFR of ESO 137-002 is 1.08 M$_\odot$/yr, from the *Galex* NUV flux density and the total *Herschel* FIR luminosity with the relation from Hao et al. (2011). If using the *WISE* 22 μm flux density and the relation from Lee et al. (2013), the estimated total SFR is 0.80 M$_\odot$/yr. The Kroupa IMF is assumed in both cases. The Lee et al. (2013) work assumed the Salpeter IMF so we multiply its SFR relation by 0.62 to convert to the Kroupa IMF. For the total amount of the molecular gas in the galaxy, $\sim 5 \times 10^9 M_\odot$, the molecular gas depletion time is ~ 5.3 Gyr, consistent with many local large spirals (e.g., Jáchym et al. 2014).

ESO 137-002 is ~ 6 times more massive than ESO 137-001 but with a comparable SF activity. The specific SFR of ESO 137-002 is ~ 7 times less than that of ESO 137-001. This is also consistent with their different $W1 - W4$ color, 4.25 for ESO 137-002 vs. 6.99 for ESO 137-001, as $W1 - W4$ is a proxy for the specific SFR. Because of the prominent bulge, ESO 137-002 is in fact a more compact galaxy than ESO 137-001.

The upstream of the galaxy is nearly dust free and gas free (Sun et al. 2010; Zhang et al. 2013) so the current SF is mainly around the nucleus and the downstream. Fig. 8 and Fig. 9 show that there is little SF in the tail. However, the disk hosts some blue star clusters with recent SF likely triggered by ram pressure (Fig. 6). The color $-$ color diagram (Fig. 7) shows that these star clusters are indeed young.

7.2 Star formation efficiency in the tail

With an upper limit of mass of M$_\star \approx 5.8 \times 10^3$ M$_\odot$ at an age of 10 Myr, the upper limit on the SFR in the tail is,

$$\text{SFR}_{\text{tail}} < \frac{5.8 \times 10^3 \text{M}_\odot}{1 \times 10^7 \text{yr}} < 5.8 \times 10^{-4} \text{M}_\odot yr^{-1} \qquad (6)$$

Since, the inner tail (002-T) of ESO 137-002 from the *APEX* data corresponds $\sim 2.2 \times 10^8$ M$_\odot$ of H$_2$. With this mass available, we estimate the gas consumption time scale as,

$$\text{SFE}_{\text{tail}} < \frac{5.75 \times 10^{-4} \text{M}_\odot \text{yr}^{-1}}{2.2 \times 10^8 \text{M}_\odot} < 2.6 \times 10^{-12} \text{yr}^{-1} \qquad (7)$$

Taking the reciprocal of the SFE, the gas depletion time in 002-T is 380 Gyr. The SFE upper limit is more than 13 times lower compared to the ESO 137-001 tail (SFE $\approx 3.6 \times 10^{-11}$ yr^{-1}) (Jáchym et al. 2014). It is also smaller than the SFE in D100's tail ($\sim 4.0 \times 10^{-12}$ yr^{-1}; note that the SFE derived in Cramer et al. (2019) is reduced by $\sim 1/3$ to account for a background source discovered by our recent *MUSE* data in D100's tail). The SFE falls with the distance from the main body to the outer tail as in the case of other RPS galaxies.

7.3 Stripping history of ESO 137-002

We can compare the amount of gas at different phases (cold molecular, warm ionized and X-ray emitting) detected in the galaxy and its tail.

- Cold molecular gas

We detected $\sim 5 \times 10^9$ M$_\odot$ of the cold molecular gas from the galaxy and at least $\sim 2 \times 10^8$ M$_\odot$ from the tail. Deeper observations plus wider coverage on the tail may reveal more cold molecular gas there. For the total stellar mass and the sSFR of ESO 137-002, the cold gas fraction of the galaxy is $\sim 20\%$ from the scaling relations by Catinella et al. (2018), although the big scatter can change the result by a factor of several. This fraction translates to $\sim 7 \times 10^9$ M$_\odot$ of the cold gas initially in the galaxy. Thus, ESO 137-002 may still retain most of its initial cold ISM, especially since the cold atomic gas is not included yet for the lack of sensitive HI data. This would suggest that the stripping is still in the early stage in ESO 137-002.

- Warm ionized gas

Zhang et al. (2013) gave a total mass of $\sim 1.9 \times 10^7$ M$_\odot$ for the Hα emitting gas in the tail, if a filling factor of 0.2% is adopted. Even the filling factor is 10 times higher, the mass only increases by 3.2 times. The mass of the warm ionized gas in the galaxy is hard to be estimated, for the contribution from star forming regions and intrinsic extinction, but it is unlikely to be comparable to the mass of the cold molecular gas.

- Hot X-ray emitting gas

Zhang et al. (2013) estimated a total mass of $\sim 2 \times 10^8$ M$_\odot$ for the X-ray emitting gas in the tail, if the filling factor is close to one. The amount of the X-ray emitting gas in the galaxy is less for the smaller volume.

Beside the total gas content, this work also reveals a strong asymmetry in the distribution of the CO gas in the disk, similar to that of the Hα and X-ray emitting gas. While the galaxy may still retain a significant portion of its initial cold ISM, the ISM distribution has been significantly modified by ram pressure and narrow stripping tails have been formed behind the galaxy.

As discussed in Sun et al. (2010) and Zhang et al. (2013), ESO 137-002 is experiencing a near edge-on stripping. This is also supported by the *HST* images of dust filaments in the disk, mostly aligned with the disk plane. The positions of young star clusters and their associated dust clouds also suggest a near edge-on stripping. On the other hand, the orientations of most dust filaments, the Hα and X-ray tails suggest a small angle of ~ 20 deg between the ICM wind direction of the disk plane. It is also noted that the secondary Hα tail also has the same orientation from the disk plane (Zhang et al. 2013). The rich dust features revealed by *HST*, including filaments and large clouds, likely disclose the distribution of the cold ISM clouds experiencing ram pressure. The complex morphologies suggest the interplay of magnetic field, galactic rotation and turbulence.

Some compact knots and clumps are observed in the galactic disk from the F275W data, revealing the presence of young star clusters (Fig. 6). They are mostly in the downstream, as the upstream has been almost completely cleaned by ram pressure. Many are on the tip of dust clouds, implying RPS triggered SF. But not all dust clouds have associated young star clusters. Since the colors of these young star clusters spread over a range (Fig. 7), it is possible that the RPS triggered SF proceeds with different timescales in different clouds so there is not a single burst-like event in the disk and some clouds do not have associated star clusters at the moment, besides the likely different intrinsic extinction for different clouds. As the ages of these young star clusters are $\sim$ several Myr - 200 Myr, ESO 137-002 would have moved for ~ 200 kpc in the sky if its velocity in the plane of the sky is 1000 km/s. Thus, the RPS triggered SF likely started when the galaxy began to plunge into the central, dense part of the cluster ICM.
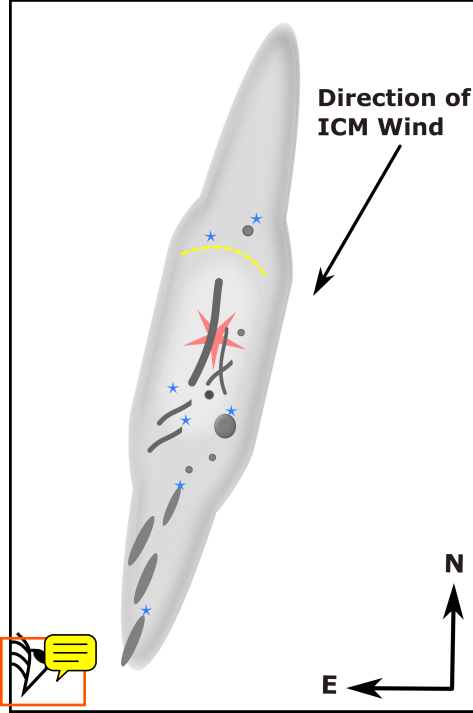
Figure 14. A cartoon representation of ESO 137-002, currently undergoing ram-pressure stripping. The ICM wind is projected to the galaxy from NW, dragging dust clouds and forming filaments at ~ 20° to the east from the south. It is likely that the ablated dust clouds are located between the bright galactic disk and us to make the dust features more significant in the optical. This is consistent with the galaxy falling to the cluster with a redshift (or moving away from us). The model depicts dark clouds, along with star clusters in blue (some at the tip of ablated dust clouds), and a strong AGN (in red) at the nuclear position, plus a yellow stripping front separating the upstream and downstream regions. Note that the stripping front is defined by the Hα and X-ray emission front, while stripping proceeds throughout the disk because the ICM is tilted relative to the disk plane (~ 20°) and the ISM is porous.

can include–stripping history,compare dust filaments and its physics, its structure, orientation with other RPS why little SF?

7.4 RPS galaxies with little SF in the stripped tail

D100 (Yagi et al. 2007; Jáchym et al. 2017), another RPS galaxy with a remarkably long and narrow Hα tail (~60 kpc) also have weak SF in the tail. The total SFR in the tail is found to be ~ 6×10^{-3} $M_\odot$ yr^{-1} (Cramer et al. 2019). Similarly, Boselli et al. (2016) studied NGC 4569, the most massive galaxy in the Virgo cluster and revealed the presence of diffuse gas tail but without any associated young stellar components. There is thus, a growing population of RPS galaxies with little SF in the stripped tails. If selected by SF tails behind the galaxy in the optical or UV (e.g., surveys like GASP or using the *Galex* data), ESO 137-002 and NGC 4569 will not be considered as a "jellyfish" galaxy. RPS galaxies with star forming trails only form a sub-group of the full population of the RPS galaxies.

In contrast, GASP galaxies are (mostly?) "jellyfish" galaxies with strong SF in the tail and/or the disk. Poggianti et al. (2017) used samples of 114 galaxies selected from different environments, masses and redshift. The majority of those galaxies show bright star-forming knots in the tails and/or disks in contrast to our results. J026, a prototype RPS galaxy in their study has SFR ~ 7 M⊙ yr^{-1}, with

90 kpc visible stripped tail. Poggianti et al. (2019) also presented an analysis of extraplanar tails of 16 RPS galaxy clusters. The SFR correlates well with gas mass and stellar mass with an average SFR ~ 1.5 —6 M⊙ yr^{-1}. Overall, the GASP galaxies correlate strongly with the Hα emissions from the young star clusters whereas in the case of ESO 137-002 as well as D100, it does not simply transact to SF. Based on the selection criteria of the GASP survey, ESO 137-002 will not be included. However, it is a RPS galaxy but not a jellyfish galaxy in stellar light. to be revised and more ...

8 CONCLUSIONS

We have presented detail analysis of ESO 137-002, a massive edge-on galaxy with a boxy bulge currently undergoing RPS. We fully employed the *HST* and the *APEX* data to constrain its age, mass, hence the SFR and efficiency. The galaxy shows signs of intense morphological disturbance mainly in the disk and the tail with numerous substructures. Using the *HST* data, we are able to resolve star clusters and constrain its SF within the disk and the tail. The inclination of the dust filaments along the line of sight and the presence of star clusters indicate that the stripping has removed most of its dust from the northwest direction. We further used the *APEX* data to inspect how much the ISM has been affected due to ram-pressure. The galaxy currently hold about 5.5×10^{10} M⊙ of cold molecular gas, distributed asymmetrically. Furthermore, it is currently falling into the potential of Abell 3627. Thus, ESO 137-002 is an RPS galaxy in the stellar light but based on the selection criteria of the GASP survey, it will not be included. Some notable features of ESO 137-002 are summarized below.

(i) The upstream of ESO 137-002 is nearly dust-free while the downstream envelops many dust features, suggesting RPS has nearly cleaned the north half of the galaxy and still continue to strip around the nucleus and the southern part. The light profile, unsharp mask image, Galfit residual image and the E(B-V) map (Fig. 4 & 5) all suggest ram-pressure as an important factor for contributing the stripping process.

(ii) Surprisingly, few blue sources (Fig. 6 & 7) are revealed in the UV filter with mostly in the downstream of the stripping front, as the upstream has already been cleaned by ram pressure. This suggests that the SF of at least some of these young star clusters is triggered by the compression of ram pressure, just like the triggered SF by SN blast waves and AGN jets.

(iii) ESO 137-002 also exhibits a hidden bar-lens feature (Fig. 3) which is supported by the presence of an X/peanut-shaped bulge. As it is currently understood that massive galaxies tend to have bar-like structures that play important role in transporting the cool gas into the hot central core, thus feeding starbursts or AGNs activities. Interestingly, it also hosts a Seyfert-2-like nucleus (Sun et al. 2010; Zhang et al. 2013)

(iv) We also aim at characterizing the properties of ESO 137-002 in the CO(2-1) and CO(3-2) frequency. Three integration points (002-C, 002-S, 002-N) on the main body and one integration point (002-T) on the tail (Fig. 11 & 12) overlapped with X-ray are selected in the CO(2-1) emission. Besides these points, two more (Fig. 13) are taken in the center and the adjacent south with the CO(3-2) emission. The corresponding molecular gas detected in the 002-C region is ~ 4.5×10^9 M⊙. Similarly, the corresponding CO(2-1) gas mass detected in the 002-S, 002-N and 002-T regions are ~ 1.0×10^9 M⊙, ~ 6.4×10^7 M⊙ and ~ 1.3×10^8 M⊙ respectively indicating asymmetric distribution in the galaxy and the tail. The